Fachtagung "Experimentelle Strömungsmechanik"
6.–8. September 2022, Ilmenau

Laservisualisierung und quantitative Auswertung des Partikeltransports von Bremsstaubemissionen

Laser visualization and quantitative analysis of particle transport from brake emission

Juan C. Londono Alfaro[1], Timo Gericke[1], Sebastian Kaiser[2]
[1] Volkswagen AG, Wolfsburg
[2] Institut für Verbrennung und Gasdynamik, Universität Duisburg Essen

Laservisualisierung, PIV, Bremsenemissionen
Laser visualization, PIV, brake emissions

Abstract

Non-exhaust emissions derived from the brake contribute to a large portion of the fine and coarse particles in the environment. Health problems have been observed to be caused by the particle pollution. The non-exhaust emissions will be regulated in the coming years. Although this phenomenon has been extensively investigated in brake test benches using ex-situ metrology systems, little is known about the sources of airborne particle and how they get transported inside the test chamber. This study uses a laser sheet and a double frame camera for the visualization of the particles emitted from a drag braking procedure. Additionally, a cross-correlation algorithm from Particle Image Velocimetry (PIV) is tested to calculate the mean velocity field of the particles and the surrounding air flow. This allows a deeper understanding of the ejection and mixture processes.

Introduction

The particulate matter from non-exhaust sources has increased over the last years due to trends like the electrification of the vehicles and the stricter regulation of exhaust emissions. Although the impact of particulate matter on human health and the environment have been investigated and guidelines have been published (World Health Organization 2021, GRPE-81-12 2020), no regulation concerning non-exhaust emissions has yet been prescribed. The incoming EU7 regulation, expected in next years, will include non-exhaust emissions, thus pressuring regulators to standardize the measurement of non-exhaust emissions and car manufacturers to lower their emissions marginally (ACEA 2021).

Non-exhaust emissions origin from the wear of brake pads, break discs, tires and the road and from the interface between tire and road, as particles might get re-suspended (Thorpe and Harrison 2008). Fig. 1 shows a diagram of the sources from non-exhaust emissions. On the car manufacturers side direct and indirect methods to reduce the non-exhaust emissions are viable. As an example, the lining of the brake pads can be optimized or low-wear brake linings can be used, such as non-asbestos organic (NAO). A further direct approach is to use coated and hardened brake discs, which wear less by induced an adhesive instead of an abrasive

GALA e.V., Karlsruhe, Germany, ISBN 978-3-9816764-8-8

braking procedure. Indirect methods consist of capturing emitted particles or enclosing the brake system, e.g., leading to the drum brake principle (Neudeck 2019).

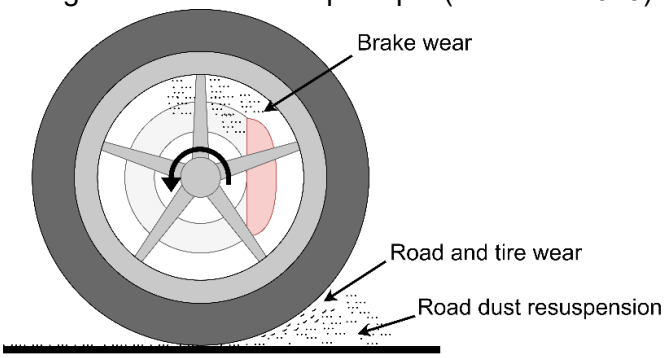

Fig. 1: Non-exhaust particle emission sources in vehicles.

Brake emissions are measured in a dynamometer, where car speed, brake pressure and the momentum are simulated. The brake is enclosed and cooled with filtered air, which transports the emitted particles to the constant volume sampling duct. Isokinetic probes are used to sample the particle laden air. A combination of several devises, like an Exhaust Engine Particle Sizer (EEPS), an Aerodynamic Particle Sizer (APS) and a Condensation Particle Counter (CPC) are used to get the particle size distribution and the number of emitted particles. This metrology systems obtain precise but averaged and delayed information from the emissions, since through the enclosure and sampling duct the particles mix, and all spatial information is lost. Fig. 2 shows a diagram of a dynamometer with the typically used ex-situ metrology.

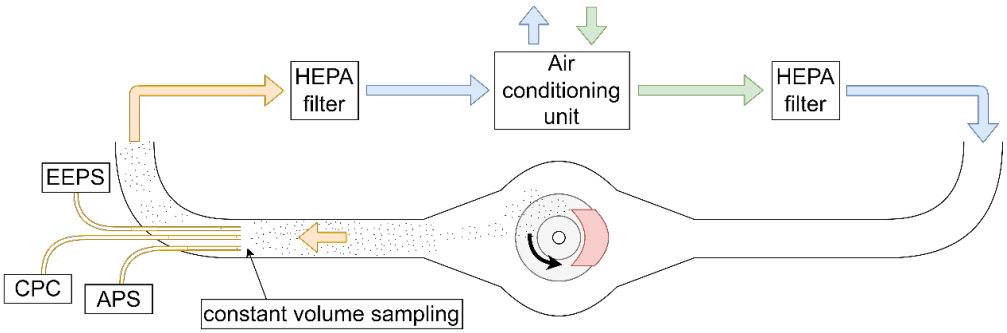

Fig. 2: Dynamometer to measure brake emissions through sampling-based particle metrology.

For both direct and indirect methods to reduce the emissions is the ex-situ measuring procedure insufficient, as more information is required to understand the underlying emission and transport mechanisms, detect and evaluate the influence of various factors on the emissions, validate numerical models and verify the performance of such methods. The information required includes the airflow conditions, the particle transport and the characterization of the particulate matter (particle size distribution and mass concentration).

For the airflow and particle transport a higher spatial resolution in two or three dimensions can be achieved with optical metrology methods, like Particle Image Velocimetry, as an ensemble of detected particles, either real emitted particle or externally seeded particles, are used to determine with a correlation algorithm the shift throughout two images with a defined time difference, thus calculating the velocity of such ensemble (Raffel and Willert 1998). This method is based on the light scattering for the detection of the particles, which in the case of brake emissions is complex, as the size of the emitted particles stretch from a couple nanometer to

GALA e.V., Karlsruhe, Germany, ISBN 978-3-9816764-8-8

several micrometers (Thorpe and Harrison 2008). This difference in orders of magnitude and the overlap between particle size and wavelength of visible light result in different types of scattering approximations depending on the size parameter $x = \pi d_p/\lambda$, where d_p is the particle's diameter and λ is the wavelength of the light (Raffel and Willert 1998):

$$x \gg 1 : \text{geometric scattering;} \quad (1)$$

$$x \approx 1 : \text{Mie scattering;} \quad (2)$$

$$x \ll 1 : \text{Rayleigh scattering.} \quad (3)$$

The reconstruction of the diameter from images used for PIV is therefore for this type of particle not feasible. Nevertheless, this method allows to measure the airflow and particle transport and evaluate the efficiency of the emissions reduction approaches (Augsburg et al. 2011, Hesse et al. 2019 and Feißel and Augsburg 2020). An investigation from Hesse (2020) studied numerically the influence of several parameters, like rotation direction of the disc, position of the caliper and cooling airflow velocity, on the particle transport inside the enclosure. It was observed that an inhomogeneous particle distribution near the brake disc establishes, as the particle trajectories are highly dependent on their diameter. Most of the small particles ($d_p \leq 1\ \mu m$) follow the stream effortlessly and are transported within the boundary layer of the rotation disc, while larger particles ($d_p \approx 10\ \mu m$) are ejected tangentially leaving the boundary layer and mixing with the main flow around the brake. An experimental validation using laser visualization and PIV was used to evaluate the numerical simulations (Hesse 2019).

As shown the laser sheet visualization of brake emission particles can answer long standing questions about how and where particles are emitted and enter the main flow. Nevertheless, for a quantitative analysis using a cross correlation algorithm to determine particle velocities might be complex, as the emission often present as a combination between disperse particles and cloud structure. The validity of such analysis will be focus on the present study based on the laser sheet visualization from multiple perspectives of a drag braking procedure.

Experimental Setup

Experiments presented in this work were conducted with the brake emissions testing system Model 3900 from the company LINK in Limburg, Germany. The enclosure was modified to allow optical access for the laser sheet and camera through two acrylic glass plates, see Fig. 5a. Two Nd:YAG single-pulse lasers Q-Smart 450 from *Quantronix* were unified for a double-pulse configuration at a wavelength of 532 nm and a frequency of 25 Hz. A laser guiding arm and a laser sheet optics, both from *LaVision*, were used to span the 1 mm thick laser sheet that was 1 mm away from the surface of the brake disc. An Imager SX 6M CMOS camera from *LaVision* with a resolution of 2752 x 2200 pixel with a maximal frequency of 12.5 Hz was used in combination with a 60 mm macro-lens with an f/2.8 aperture. The image size was 190 x 151 mm with a scale factor of 14.5 pixel/mm for the lateral perspective and was 143 x 115 mm with a scale factor of 19.22 pixel/mm for the frontal perspective. The two camera positions are shown in Fig. 5b and 5c.

A drag braking procedure was performed to record the images, where the velocity and braking pressure were kept constant at 130 km/h and 30 bar, respectively. This allows to draw an average over the recordings, as only the temperature increases during the braking procedure. A vented disc brake with ECE brake pads and a single cylinder was used. The bedding of the

GALA e.V., Karlsruhe, Germany, ISBN 978-3-9816764-8-8

brake couple was performed with five WLTP brake cycles. The brake caliper was positioned at 3 o'clock to ensure an optical access for the laser sheet to the region after the brake pad, as the rotation was in counterclockwise direction. The volume flux of the cooling air was kept at 475 m³/h. During the experiments the cooling air was at a temperature of 20 ± 0.9 °C and a relative humidity of 50 ± 3.8 %. The start disc temperature was set to 100°C and the braking duration was set to 7.4 s. A total of 394 images from seven drag breaking procedures were used for the analysis. The time delay between the double-frame images was 30 µs. Flow measurement using DEHS as seeding particles were performed, in which 2000 images were recorded with a time delay of 50 µs. During the flow measurement the brake was not activated leaving a gap between brake pad and brake disc. The deviation of the measured to the real airflow during the drag braking cannot be quantized. Computational fluid dynamic simulations might help to perform this evaluation.

The synchronization between the laser and the camera was performed by a programmable timing unit (PTU) and the software DaVis 10.2 from *LaVision*, which was also used to perform the analysis of the recordings and calculate the vector fields. After an image preprocessing, where unwanted regions are masked, the background subtracted and a normalization of the illumination across the image is conducted, a multi-pass PIV algorithm was used with an interrogation window of 96x96 pixel and 24x24 pixel at 75% overlap. For the DEHS measurements a single pass with an interrogation window of 24x24 pixel with an overlap 75%. Afterwards, an average velocity field is computed. Additionally, the cloud structures were separated from the dispersed particles and analyzed with a multi-pass algorithm with an interrogation window of 128x128 pixel and 64x64 pixel at 75% overlap.

Additionally, the particle ex-situ metrology consisting of a CPC, EEPS and APS were used to record the emissions at a rate of 1Hz.

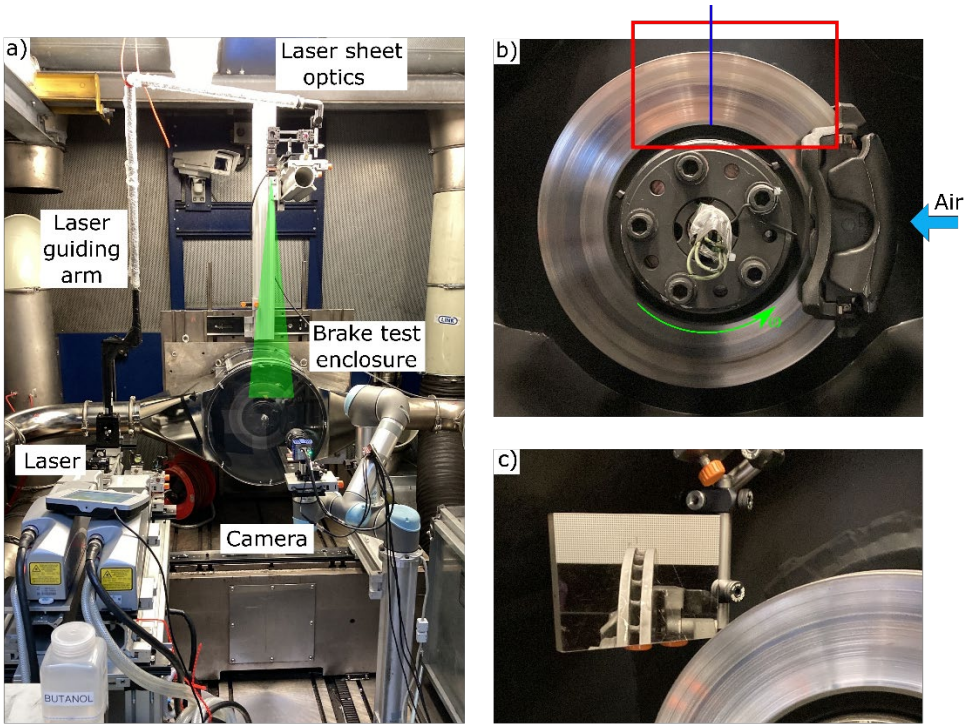

Fig. 5: a) PIV experiment setup at the brake emissions dynamometer. Two acrylic glass windows from the frontal and upper side ensure the optical access for the laser sheet and camera. b) Camera perspective from the side (red) and from the front through a mirror (blue). c) Position of the mirror for frontal camera perspective. Cooling air flows from right to left. Rotation of the brake disc in counter-clockwise direction.

GALA e.V., Karlsruhe, Germany, ISBN 978-3-9816764-8-8

Results

From the recorded images the braking procedure can be displayed in a sequence of images, as shown in Fig. 6a-f for the lateral perspective and Fig. 6g-l for the frontal perspective. Slight variations within the tribological system due to inhomogeneity of the brake pad or velocity and brake pressure regulation uncertainty lead to unique braking procedures. The displayed image sequences were matches to show similar phenomena although the recording time might not match. After pressure is applied and the piston threshold of 5 bar is surpassed a dense cloud of emissions is ejected. After that initial phase the emissions stabilize, as the disc rotation and brake pressure are kept constant. Within this period of constant emissions an averaging of the particles locations and trajectories can be performed. A second dense cloud is noticed at the end of the braking procedure. A similar phenomenon has been observed by Hagino et al. 2015, where the emissions during and after the braking procedure were measured. They observed that in a braking with an initial velocity of 60 km/h and a deceleration of 1,5 m/s² between 22% and 55% of the PM emissions originated from the acceleration after the braking procedure. An explanation for this delayed emission has be given by Park et al. 2021. They studied the wear based emissions from low-steel and no-steel brake pads with the WLTP cycle and observed that due to the topology of low-steel pads, consisting of hard plateaus and lowlands, the particles agglomerate and get compacted in the lowlands and get airborne after the brake is released. Not only the absence from pressure but also the influence of the newly developed boundary layer and the centrifugal force might lead to this detachment. The emission factor and the brake disc temperature are plotted over the time for all individual braking procedures as well as the average in Fig. 6n. The particle size distribution is plotted over the time in Fig. 6m.

Apart from the qualitative analysis the double-frame images also allow to analyze the trajectories if an ensemble of particles in a qualitative manner with a cross-correlation algorithm, commonly used in PIV. The algorithm compares the shift of interrogation window with an user-defined size to estimate the best fit for the shift between frames. A raw image and its corresponded processed images from a drag braking are shown in Fig. 7a-b. Through the image processing the background is subtracted and the over-illuminated regions (colored in red) are ignored. This improves the analysis as the optimal correlation should be punctual and unambiguous. This needs to be examined carefully as structures might lead to false vector detection, as there is no punctual correlation but rather a lineal or a surface. A processed image with only the cloud structures is shown in Fig 7c. A correlation with a 96x96 pixel interrogation window from a region with a cloud structure and from a region with dispersed particles (green rectangles in the raw image) are displayed in Fig. 7e. The resulting average vector field are presented in Fig. 7f-g. A processed image and the vector field from the airflow measurement using DEHS are shown in Fig. 7d and 7h.

To evaluate the quality of the analysis of the cloud structures the velocity field from the all emitted particles will be used as reference (Fig. 7f). It needs to be mentioned, that the displayed velocity represent the ensemble velocity and not the individual particle velocity. As described by Hesse 2020 the trajectory and velocity of an individual particle depends on its diameter. Since the particles diameter were not detected and analyzed separately, an averaging across the individual particles velocity was performed. From Fig. 7g it can be noticed that the velocity of the structures seems to be overappreciated in the outer part of the disc. A possible reason is the elongated correlation that arise due their form. This might difficult the determination of

GALA e.V., Karlsruhe, Germany, ISBN 978-3-9816764-8-8

the real shift. Thus, it would be advisable to avoid through proper image processing the analysis of such structures in further investigations.
A further comparison can be drawn between the velocity field of the emitted particles and the surrounding air. It can be appreciated that near the brake disc the particle move with a higher velocity that the air and have a higher tangential velocity. When particles detach from the surface of the brake disc, they are ejected at the tangential velocity of the rotating disc, which is 8.7 m/s and 17.4 m/s for the inner and outer border of the disc, respectively. As soon as the particles enter the boundary layer, they are slowed down. Through the higher radial velocity of the flow the particles are transported toward the outer border and enter the main flow. This transport mechanism can be highly influenced by the position of the caliper, cooling airflow and geometry of the disc.

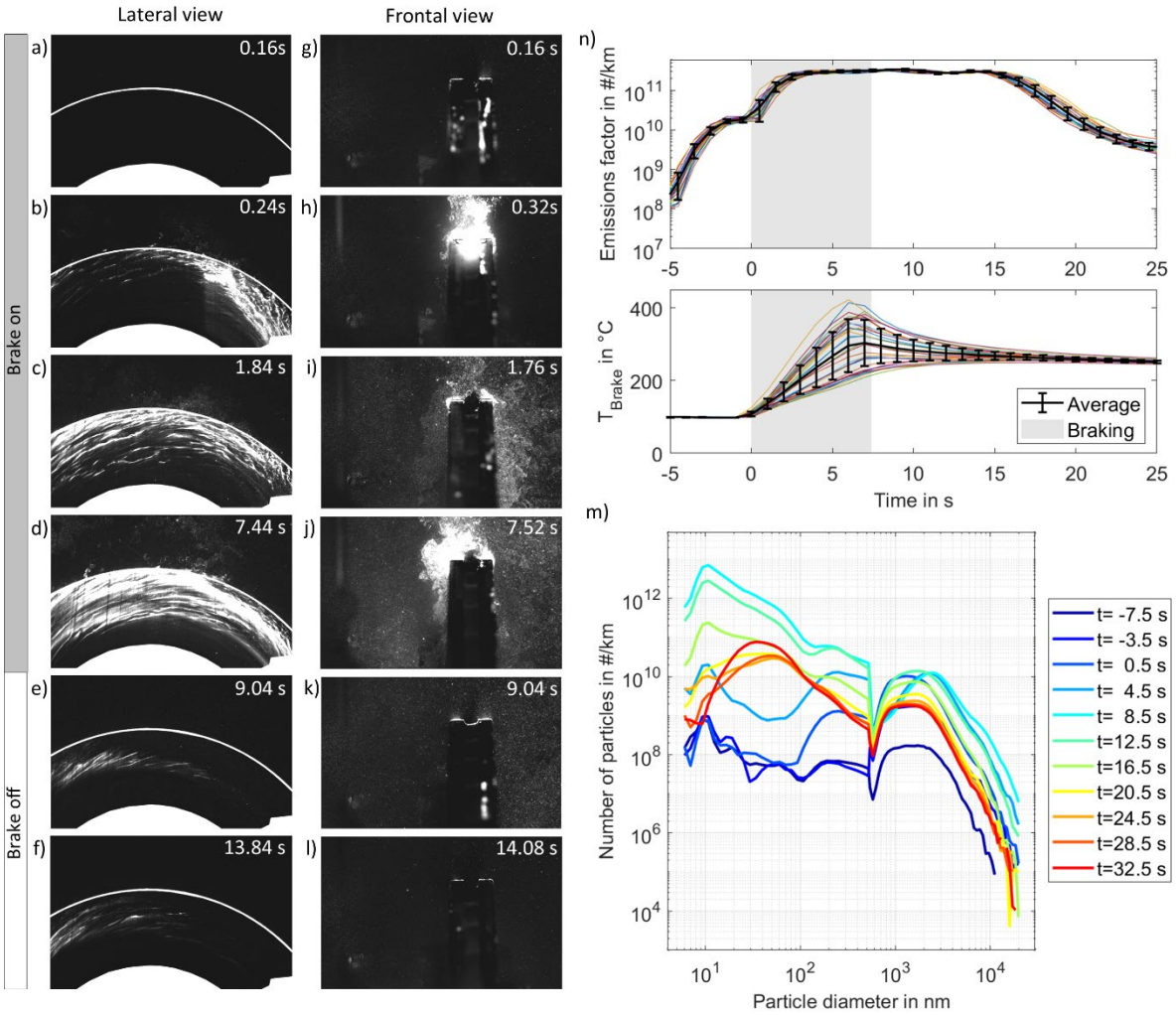

Fig. 6: a-f) Image sequence for a drag braking from the lateral camera perspective. g-l) Image sequence for a drag braking from the frontal camera perspective. n) Individual and averaged emissions factor and brake disc temperature over time. The gray area represent the braking procedure. m) Particle size distribution over time.

GALA e.V., Karlsruhe, Germany, ISBN 978-3-9816764-8-8

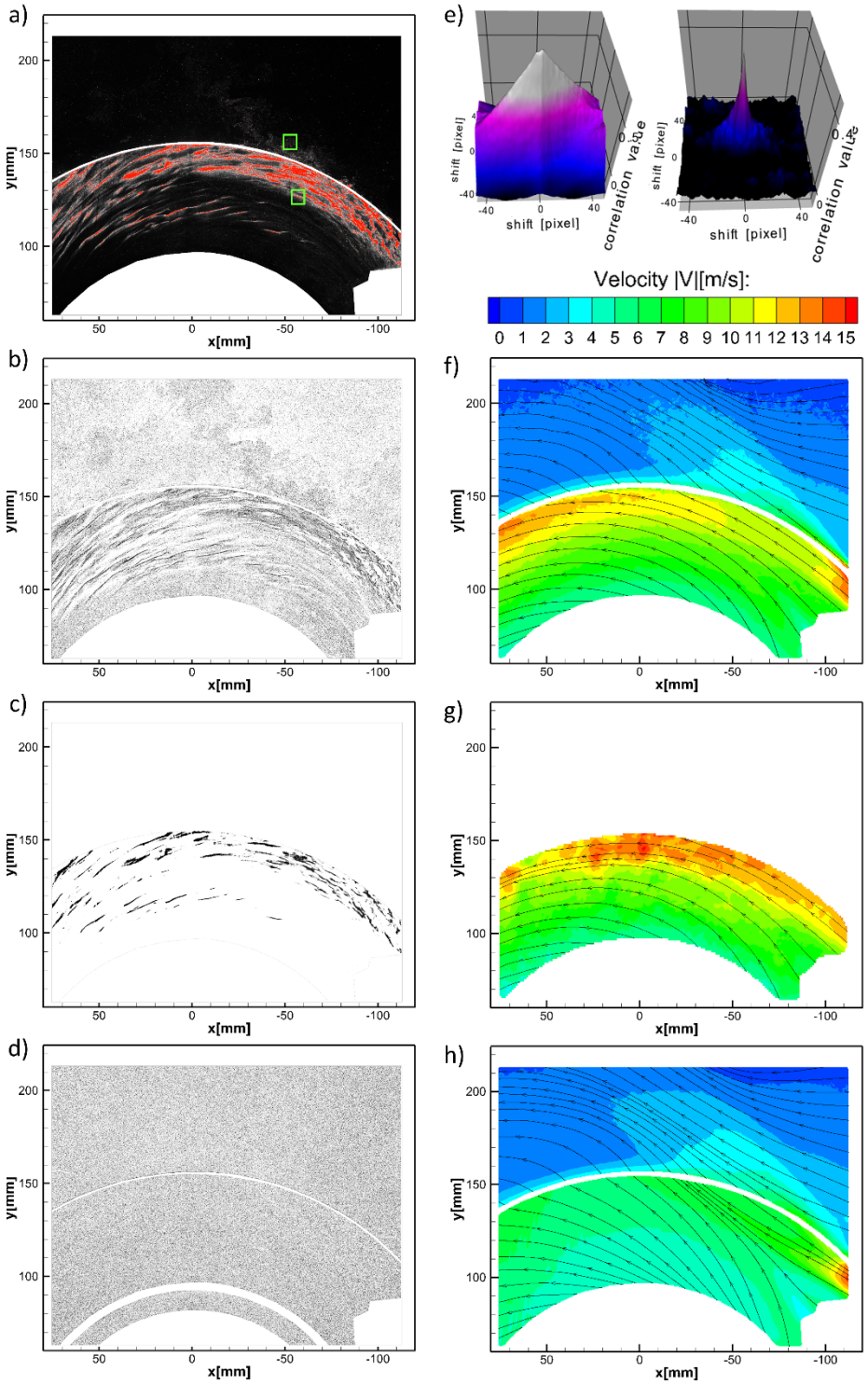

Fig. 7: a) Raw image from drag braking with red color marking the over-illuminated (threshold 4096 counts) areas, mostly from particle cloud structure. b) Processed image from drag braking for PIV analysis. c) Processed image from drag braking with only cloud structures. d) Processed image from flow measurement with DEHS. e) Correlation peaks from a cloud structure (left) and a disperse particle region (right) as shown in green rectangle in the raw image. f) Average velocity field from ensemble of particles emitted from a drag braking. g) Average velocity field from the cloud structures during the drag braking. h) Average velocity field from airflow with gap between brake pad and brake disc.

GALA e.V., Karlsruhe, Germany, ISBN 978-3-9816764-8-8

Conclusion

In the present paper the brake emissions near the brake disc have been visualized with a laser sheet. The recorded images were used to perform a qualitative analysis, which together with recorded data from particle sizers and a particle counter, confirmed time resolved behavior of the emissions observed in other studies. This method proofs to be a helpful instrument in order to understand the ejection and mixing behavior of the particles. Furthermore, a quantitative analysis of the double-frame images was performed with a cross-correlation algorithm from PIV. A special care has to be taken with dense particle cloud structures, as the resulting elongated correlation might lead to an overestimation of the velocity. Through a measurement of the averaged particle velocity from an ensemble of particles emitted from a drag braking procedure and the surrounding airflow using DEHS a deeper understanding regarding the transport and mixing mechanism can be achieved.

The results, opinions and conclusions expressed in this publication are not necessarily those of Volkswagen Aktiengesellschaft.

Acknowledgement

The authors would like to thank Prof. Sebastian Kaiser from the University Duisburg-Essen and the colleagues from the brake development department at VW.

Literature

ACEA (2021). "ACEA Proposal for Euro 7", European Automobile Association, Retrieved February 8, 2022, from https://www.acea.auto/

Alemani, M., Wahlström, J., & Olofsson, U. (2018). On the influence of car brake system parameters on particulate matter emissions. *Wear*, *396*, 67-74.

Augsburg, K., Gramstat, S., Horn, R., & Sachse, H. (2011). Measures development for brake dust emissions with computational fluid dynamics and particle imaging velocimetry (No. 2011-01-2345). SAE Technical Paper.

Feißel T., Augsburg, K. (2020). Analytical investigation of tire induces particle emissions. FISITA 2020 World Congress, Prage, Czech Republic.

GRPE-81-12 (2020). Non-Exhaust Brake Emissions — Laboratory testing — Part 1: Inertia Dynamometer Protocol to Measure and Characterise Brake Emissions Using the WLTP-Brake Cycle. Particle Measurement Program (PMP) from Working Party on Pollution and Energy (GRPE), 81st GRPE, 9-11 June 2020

Hagino, H., Oyama, M., & Sasaki, S. (2015). Airborne brake wear particle emission due to braking and accelerating. *Wear*, *334*, 44-48.

Hesse, D., Augsburg, K., Feißel, T., & Sommer, J (2019). Real driving emissions measurement of brake dust particles. Eurobrake 2019, Dresden, Germany.

Hesse, D. (2020). Beitrag zur experimentellen und analytischen Beschreibung partikelförmiger Bremsenemissionen (Doctoral dissertation, TU Ilmenau).

GALA e.V., Karlsruhe, Germany, ISBN 978-3-9816764-8-8

Neudeck, D. (2019). Low emission brakes–can the friction brake still be saved?. In *9th International Munich Chassis Symposium 2018* (pp. 675-687). Springer Vieweg, Wiesbaden.

Park, J., Joo, B., Seo, H., Song, W., Lee, J. J., Lee, W. K., & Jang, H. (2021). Analysis of wear induced particle emissions from brake pads during the worldwide harmonized light vehicles test procedure (WLTP). *Wear*, *466*, 203539.

Raffel, M., Willert, C. E., & Kompenhans, J. (1998). Particle image velocimetry: a practical guide (Vol. 2). Berlin: Springer.

Thorpe, A., & Harrison, R. M. (2008). Sources and properties of non-exhaust particulate matter from road traffic: a review. Science of the total environment, 400(1-3), 270-282.

World Health Organization (2021). WHO global air quality guidelines. Particulate matter (PM2.5 and PM10), ozone, nitrogen dioxide, sulfur dioxide and carbon monoxide.", Geneva

GALA e.V., Karlsruhe, Germany, ISBN 978-3-9816764-8-8